Communications in Physics, Vol. 29, No. 3 (2019), pp. 277-284
DOI:10.15625/0868-3166/29/3/13831

SIMULATION FOR OPTIMIZING THE DESIGN OF CRYOGENIC STOPPING CELL FOR THE IGISOL FACILITY AT ELI-NP

LE TUAN ANH[1,†] PHAN VIET CUONG[2], P. CONSTANTIN[3], B. MEI[3], D. L. BALABANSKI[3], NGUYEN HONG HA[4], HO THI THAO[4], KIM TIEN THANH[4] NGUYEN THE VINH[5], PHAM DUC KHUE[6] AND HOANG HUU DUC[7]

[1]*Graduate University of Science and Technology, Vietnam Academy of Science and Technology*

[2]*Research and Development Center for Radiation Technology, Vietnam Atomic Energy Institute*

[3]*Extreme Light Infrastructure – Nuclear Physics, "Horia Hulubei" National Institute for Physics and Nuclear Engineering, Str. Reactorului 30, 077125 Bucharest Magurele, Romania*

[4]*Centre of Nuclear Physics, Institute of Physics, Vietnam Academy of Science and Technology*

[5]*Vietnam Atomic Energy Institute*

[6]*Institute for Nuclear Science and Technology*

[7]*Centre for Technology Environmental Treatment, Ministry of Defence, Hanoi, Vietnam*

[†]*E-mail:* letuananh.nuclphys@gmail.com

Received 20 May 2019
Accepted for publication 16 July 2019
Published 15 August 2019

Abstract. *The production of the exotic neutron-rich ion beams from photofission of the actinide targets in an IGISOL facility will be studied via an experimental program that will take place at the Extreme Light Infrastructure - Nuclear Physics (ELI-NP) facility. Geant4 simulation toolkit was used for optimizing the target configuration in order to maximize the rate of released photofission fragments from targets placed in a cell filled with He gas.*

Keywords: ELI-NP, Photofission, Gas cell, IGISOL, Radioactive ion beam.

Classification numbers: 23.90.+w, 25.85.Jg.

I. INTRODUCTION

Extreme Light Infrastructure (ELI) is one of the 48 infrastructures of the European Strategy Forum for Research Infrastructure (ESFRI) [1] . ELI-NP facility, which is one of the three laboratories of the ELI [1, 2], has the mission to promote nuclear physics studies with a laser-driven

electron, proton or heavy-ion beams, and especially with a brilliant γ beam. This γ beam is obtained by Compton backscattering (CBS) of a laser beam on an intense electron beam accelerated by a linear accelerator [3]. This gamma beam will be highly polarized (>99%) and have a high spectral density of up to 4.10^4 photons/s/eV in the energy range of 0.2-19.5 MeV with a bandwidth of 0.3-0.5%.

Because of having energy range which covers the whole Giant Dipole Resonant of Uranium and Thorium isotopes [4], the ELI-NP gamma beam is suitable for the production of the exotic neutron-rich photofission fragments.

To form the radioactive beam from photofission fragments, an ion-guide isotope separation on-line (IGISOL) facility will be constructed at ELI-NP. The gamma beam impinging on Uranium thin foils placed in the center of a Cryogenic Stopping Cell (CSC) will induce photofission. The ions diffusing into the gas from the thin foils will, then, be drifted out by a strong DC field in the orthogonal direction. When these ions reach close to the cell wall, a resonant RF fields will push them towards the exit nozzle where they are taken out in a supersonic jet by a gas flow.

In this paper, simulations with Geant4 toolkit were performed for optimizing some basic parameters for the development of CSC prototype for IGISOL facility at ELI-NP.

II. LASER COMPTON BACK SCATTERING AT ELI-NP

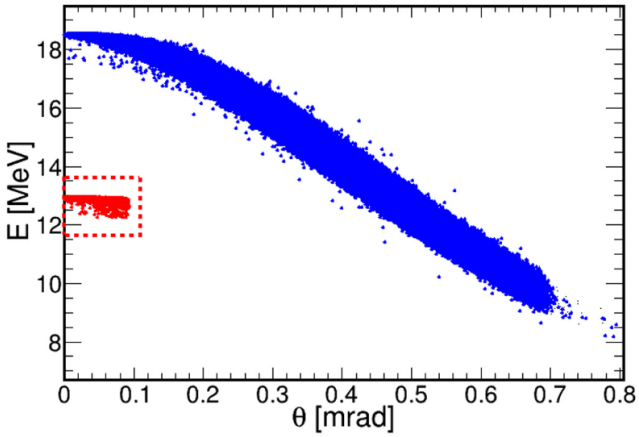

Fig. 1. Energy-angle correlation for two gamma beams: a broad beam up to 18.5 MeV collimated below 0.7 mrad (blue) and a pencil beam up to 12.9 MeV collimated below 0.09 mrad (red) [5].

The ELI-NP gamma beam will be produced through Compton Backscattering of a laser beam on an intense accelerated electron beam. CBS can be considered as a "photon accelerator". More details of CBS were presented in [3]. The energy which a photon with the initial energy E_L obtained after scattering off a relativistic electron with the kinetic energy T_e is approximately calculated as:

$$E(\theta, T_e) = \frac{4\gamma^2{}_e E_L}{(1+\delta^2/4+a^2{}_{0p}/2)+\gamma_e^2\theta^2} \quad (1)$$

where θ is the photon scattering angle and $\gamma_e = 1 + \frac{T_e}{m_e c^2}$ is Lorentz factor of accelerated electron. ELI-NP gamma beam uses green laser with E_L=2.4 eV, the laser incident angle $\delta = 7.5^o$ and laser parameter $a_{0p} = 0.041$ [5]. Eq.(1) implies that by using a suitable collimator placed at certain θ angle, one can select the energy of gamma beam. The maximum energy which a scattered photon can gain is achieved in head-on collisions. With the above set of parameters, the maximum energy is given by:

$$E_\gamma{}^{max}(T_e) = 9.55eV(1 + \frac{T_e}{m_e c^2})^2 \quad (2)$$

where m_e is the rest mass of the electron and c is the speed of light.

Figure 1 presents the two types of γ beams that will be produced at ELI-NP by using suitable collimator. This figure is obtained through Geant4 simulation. The broad beam marked by blue dots has the energy range from 10 MeV to 18.5 MeV. This broad beam, which obtained by setting T_e = 720 MeV and collimating the beam below 0.7 mrad, will be used for photofission.

III. THE IMPLEMENTATION OF GEANT4 CODE FOR OPTIMIZING THE DESIGN OF GAS CELL AT ELI-NP

Geant4 Monte Carlo simulation framework [6] is dedicated to the simulation of particles through matter. In our work, the Geant4 code was implemented to help in giving a conceptual design of future CSC, as well as studying setup for other future experiments at ELI-NP.

III.1. Simulation of photofission process in Geant4

To describe a process in Geant4, two mandatory modules must be implemented. The first one controls the calculation of reaction cross-section, while the other determines the final states of out-going particles and residual nucleus.

For the first module implementation, the ^{238}U photofission cross-section was calculated by the parametrization obtained by using the experimental data measured by Caldwell *et al.* [4], Ries *et al.* [7], and Csige *et al.* [8]. Figure 2 shows the comparison between the parametrization and experimental data. More details for this empirical parametrization were presented in our publication [9]. This parametrization is implemented into a new class which inherited from Geant4 class G4VCrossSectionDataSet.

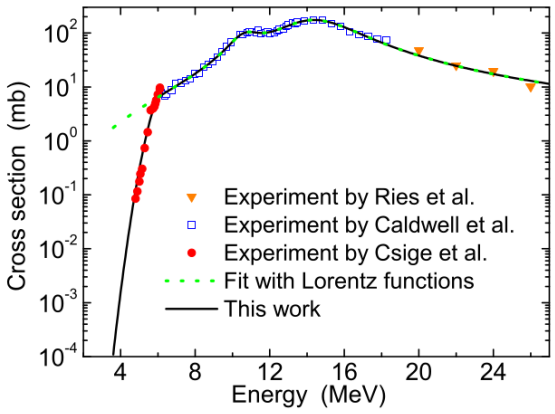

Fig. 2. The 238U photofission cross sections measured by Caldwell *et al.* [4], Ries *et al.* [7], and Csige *et al.* [8], as a function of the incident photon energy. The full line indicates calculations by the parametrization developed by our work in [9].

The second module controls which particles will be created and their kinematics. This module includes two parts. The first part relates to what kind of fragments and particles will be created in the photofission. The parametrization presented in our publication [9] was implemented

into Geant4 for this job. Figure 3 shows the yields calculated by the parametrization (the red line) in comparison with experimental data measured by Donzaud *et al.* [10] and Pellereau *et al.* [11]. The second part of the second module generates the kinematics of photofission fragments using total kinematics energy data from [12, 13] and energy and momentum conservation laws.

III.2. Ion stopping process in Geant4

After being generated, the photofission fragments propagate inside the ^{238}U target and lose their kinetic energy. Some of the fragments will lose all their kinetic energy and stop inside the foils. Meanwhile, the others will be released into the gas, and continue to be slowed down by the gas. The transport of fragments inside target and gas is handled by Geant4 classes for low energy electromagnetic interactions, including the electronic and nuclear ion stopping and multiple scattering effects.

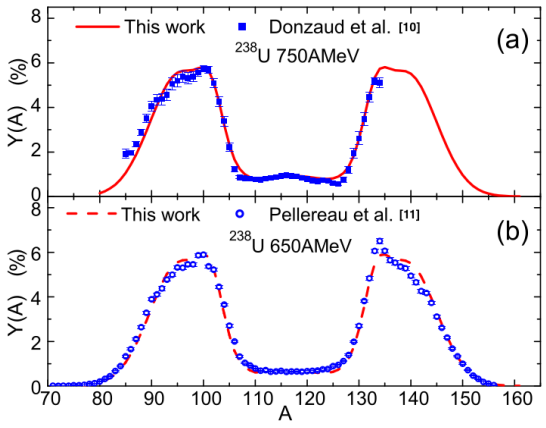

Fig. 3. Comparison between the mass yields measured in two experiments at GSI via the virtual photon induced fission of 238U [10, 11] and those calculated by the parametrization developed by our work in [9].

The energy loss by ionization is described by the well-known Bethe–Bloch formula in which the ionic charge q is assumed to be constant during stopping process. This assumption is satisfactory for the ions which have large velocity and low nuclear charge because all of their electrons will be quickly stripped out. In general, however, q fluctuates during ion stopping process in matter due to the competition between ionization and electron capture processes [5]. Geant4 uses the ionic effective charge formalism from Ziegler and Manoyan [14] to describe the evolution of q. In our work, another q-parametrization developed by Schiwietz and Grande [15] is implemented into Geant4 in order to have a comparison with Ziegler-Manoyan q-parametrization.

IV. TARGET GEOMETRY OPTIMIZATION

The future CSC will be installed at two considered locations at distance D =7 m and 40m from the γ origin. Figure 4 shows the target configuration inside the gas cell. The γ beam propagates along the positive z-axis. The tilting foils are placed along the γ beam. The fragments from photofission of ^{238}U released from these foils will be slowed down transversally in the gas and drifted by a direct current (DC) field. With the fixed number of foils N, the release rate, Nr, depends on the transversal size A, the tilting angle a and the foil thickness t.

The transversal size A should be set equal to the beam spot size for optimizing the number of photofission occurring in ^{238}U foils. The beam spot size, and then A, can be estimated as follows:

$$A = 2D\theta = 4D\sqrt{E_l/E_{th} - E_L/E_\gamma^{max}} \quad (3)$$

where $E_L = 2.4$ eV is the laser photon energy and E_{th} is the energy threshold. In the case of ELI-NP range of γ-ray emission angle $\theta < 1$ mrad , the small angle approximation $\tan(\theta) \approx \sin(\theta) \approx \theta$ is used. In the rest of this work, the maximum fragment release rate N_r is optimized for $E_{th} = 12$ MeV and $E_{max} = 17$ MeV.

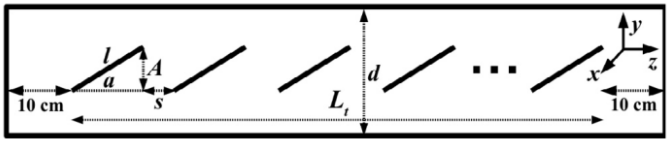

Fig. 4. The yz-plane of the target geometry inside the gas cell. The gamma beam propagates along the z axis and the DC field drifts ions along the x axis.

The transversal size A, the tilting angle a, and the number of foils N affect the total length L_t as following:

$$L_t = \frac{NA}{tan(a)} + (N-1)s \tag{4}$$

where s is the inter-foil distance. The value s should be zero so that the number of foils N gets the maximum value. Thus, Eq. (4) is rewritten:

$$L_t = \frac{NA}{tan(a)} \tag{5}$$

Because of the space constraints at the first CSC location, the target length is fixed at its maximum value $L_t = 1$ m [16]. Meanwhile, $L_t = 2$ m is chosen for the second location.

The dependence of photofission rate and release rate on the foil thickness are presented in Fig. 5 for $L_t = 1$ m, $A = 6$ mm and $a = 10^\circ$, leading to $N = 30$. The black circles stand for photofission rate, while the squares are for release rate. The shape of the photofission rate implies that the photofission rate increases proportionally with the increase of t.

The release rate N_r, however, increases quickly and reaches saturation after a certain foil thickness. This means that any increase above this value leads to an increase of the mass of ^{238}U used, without a gain in the rate of released fragments. Hence, the background related to pair production $\gamma \rightarrow e^+e^-$ in the target foils would increase. Saturation is met with $t > 1\mu$m for the Schiwietz-Grande q-parameterization [15] expressed by blue

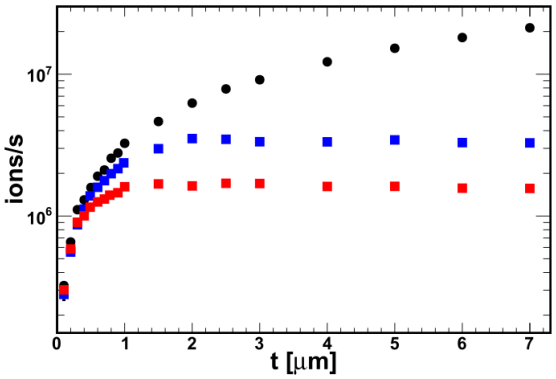

Fig. 5. The dependence on the ^{238}U foil thickness t of the photofission rate with black circles and of the fragment release rate using different q-parameterizations: Schiwietz- Grande [15] in red and Ziegler-Manoyan [14] in blue. The maximum release rate was found to be in the range of 10^6 to 10^7 ions/s.

squares and $t > 2\mu$m for the Ziegler-Manoyan q-parameterization [14] marked with red squares in Fig. 5. The optimal foil thickness is $t \approx 2\mu m$. This value remains approximate when the other target geometry parameters change [16].

The release rate depends weakly on the tilting angle a. A series of simulations were done by changing the value of a, and the results showed that the distribution in Fig. 5 goes down by 2% and increases by 5% when a is changed by 10°, respectively. However, the tilting angle may relate to the loss of released fragments by hitting neighboring foils. This loss increases fast at large a: from 1% at 5°, to 3.5% at 15°, to 24% at 45°. The 3.5% efficiency loss is considered acceptable, i.e. $a = 15^\circ$ is the optimal choice.

There is another parameter which also affects the release rate. This parameter is the backing thickness B. The backing is the thin layers of graphite covering the ^{238}U foil for supporting. When the fragments travel inside the graphite layer, some of them will lose energy and stay inside the backing layer. This leads to a decrease of the fragments entering the gas. The level of loss depends on the thickness of the backing layer. To optimize the backing thickness, the quantity $P_B(\%)$ is used:

$$P_B = \frac{\text{Number of ions lost in the backing layers}}{\text{Number of ion released from } ^{238}U \text{ foils}} \tag{6}$$

Figure 6 shows the dependence of the loss fraction P_B on backing thickness for both Schiwietz-Grande and Ziegler-Manoyan q-parameterizations. If P_B = 5% marked by dash line is acceptable, then the optimal value for backing thickness can be in the range 0.4 - 0.9 μm.

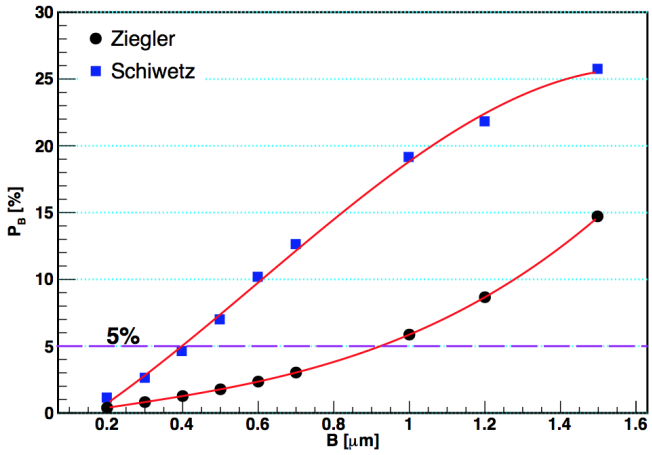

Fig. 6. The dependence of P_B on the backing foild thickness.

V. STOPPING LENGTH OF RELEASED FRAGMENTS IN GAS

After releasing out of the target foils, the photofission fragments travel and stop in the He gas. Studying the stopping length will help to optimize the width of the CSC, i.e. the parameter d in Fig. 4. The maximum extraction efficiency of ion in He gas has been observed [17] in the temperature range between 60 K and 90 K. The gas pressure values below 300 mbar are

considered, accordance with expected limitations of RF carpet functionality [18]. The stopping length, L, depends on the He gas configurations. Three sets of temperatures and pressures of He gas are used for studying L: A (T = 90 K, P = 100 mbar), B (T = 80 K, P = 200 mbar), C (T = 70 K, P = 300 mbar). The corresponding density of these three sets are $\rho_A = 0.053$ mg/cm^3, $\rho_B = 0.120$ mg/cm^3, and $\rho_C = 0.206$ mg/cm^3, respectively.

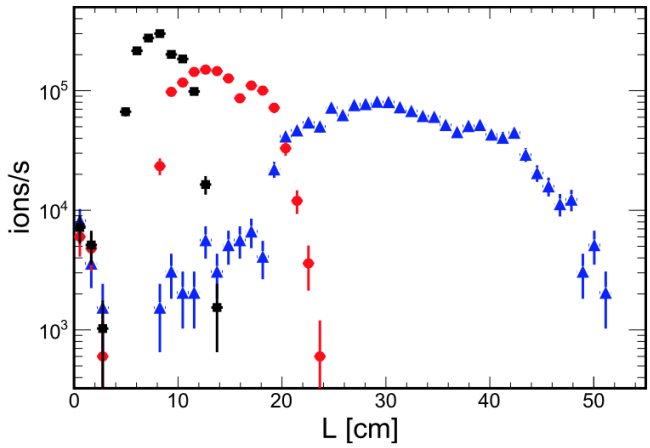

Fig. 7. Stopping length for various densities of the He gas: ρ_A = 0.053 mg/cm^3 (blue triangles), ρ_B = 0.120 mg/cm^3 (red circles) and ρ_C = 0.206 mg/cm^3 (black squares).

Figure 7 shows the fragment stopping length distributions corresponding to each of the above gas parameter sets. The maximum stopping length, L_{max}, which is the path-length at which 95% of the fragments have stopped, is used for determining the width of CSC. L_{max} = 43.7 cm is found for the parameter set A. Meanwhile, L_{max} = 19.4 cm, and L_{max} = 11.3 cm are found for B and C, respectively. In all cases, the following relationship is found:

$$\rho L_{max} = 2.33 \text{ mg/cm}^2 \tag{7}$$

The width of the CSC can be slightly set above $d \approx 2L_{max}$. For instance, if the cell operates at 100 mbar and 90 K, its width would be $d = 88$ cm.

VI. CONCLUSIONS

An implementation of Geant4 simulation toolkit was used for optimizing the target geometry of CSC at ELI-NP. The optimal value for ^{238}U foil thickness is t $\approx 2\ \mu m$. The tilting angle has a small effect on the release rate, but it has an impact on the loss of released fragment by hitting neighboring foils. The optimal value is found to be 15° for a. The presence of graphite backing layers introduces the loss of fragments by stopping inside these layers. The backing thickness should be chosen in the range from 0.4 μm to 0.9 μm to hold $P_B \approx 5\%$. The maximum release rate was found to be in the range of 10^6 to 10^7 photofission fragments per second. The width of the CSC should be slightly longer than the value $2L_{max}$, i.e. depending on the He gas configurations, the parameter d can be determined.

ACKNOWLEDGMENT

This work was supported by the Extreme Light Infrastructure Nuclear Physics Phase II, a project co-funded by the Romanian Government and the European Union through the European Regional Development Fund's Competitiveness Operational Programme (1/07.07.2016, COP, ID 1334). Phan Viet Cuong and Le Tuan Anh acknowledge the support from the Vietnam Academy of Science and Technology under Grant No. VAST. CTVL.03/17-18.

REFERENCES

[1] N. Zamfir, *EPJ Web of Conferences* **66** (2014) 11043.
[2] D. Balabanski, *Journal of Physics: Conference Series* **590** (2015) 012005.
[3] O. Adriani, S. Albergo, D. Alesini, M. Anania, D. Angal-Kalinin, P. Antici, A. Bacci, R. Bedogni, M. Bellaveglia, C. Biscari et al., *arXiv preprint arXiv:1407.3669* (2014) .
[4] J. T. Caldwell, E. J. Dowdy, B. L. Berman, R. A. Alvarez and P. Meyer, *Phys. Rev. C* **21** (1980) 1215.
[5] P. Constantin, D. L. Balabanski and P. V. Cuong, *Nucl. Instr. and Meth. B* **372** (2016) 78.
[6] S. Agostinelli, J. Allison, K. a. Amako, J. Apostolakis, H. Araujo, P. Arce, M. Asai, D. Axen, S. Banerjee, G. . Barrand et al., *Nucl. Instr. and Meth. A* **506** (2003) 250.
[7] H. Ries, G. Mank, J. Drexler, R. Heil, K. Huber, U. Kneissl, R. Ratzek, H. Ströher, T. Weber and W. Wilke, *Phys. Rev. C* **29** (1984) 2346.
[8] L. Csige, D. Filipescu, T. Glodariu, J. Gulyás, M. Günther, D. Habs, H. Karwowski, A. Krasznahorkay, G. Rich, M. Sin et al., *Phys. Rev. C* **87** (2013) 044321.
[9] B. Mei, D. Balabanski, P. Constantin, L. Anh and P. Cuong, *Phys. Rev. C* **96** (2017) 064610.
[10]
[11] E. Pellereau, J. Taïeb, A. Chatillon, H. Alvarez-Pol, L. Audouin, Y. Ayyad, G. Bélier, J. Benlliure, G. Boutoux, M. Caamaño et al., *Physical Review C* **95** (2017) 054603.
[12] S. Pommé, E. Jacobs, M. Piessens, D. De Frenne, K. Persyn, K. Govaert and M.-L. Yoneama, *Nuclear Physics A* **572** (1994) 237.
[13] M. Piessens, E. Jacobs, S. Pommé and D. De Frenne, *Nuclear Physics A* **556** (1993) 88.
[14] J. Ziegler and J. Manoyan, *Nucl. Instr. and Meth. B* **35** (1988) 215.
[15] G. Schiwietz and P. L. Grande, *Nucl. Instr. and Meth. B* **175** (2001) 125.
[16] P. Constantin, D. L. Balabanski and P. V. Cuong, *Nucl. Instr. and Meth. B* **397** (2017) 1.
[17] P. Dendooven, S. Purushothaman and K. Gloos, *Nucl. Instr. and Meth. A* **558** (2006) 580.
[18] M. Ranjan et al, *Eur. Phys. Lett.* **96** (2011) 52001.